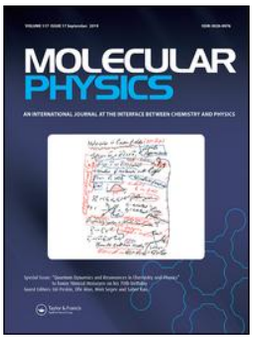

Taylor & Francis
Taylor & Francis Group

Molecular Physics

An International Journal at the Interface Between Chemistry and Physics

ISSN: 0026-8976 (Print) 1362-3028 (Online) Journal homepage: https://www.tandfonline.com/loi/tmph20

Atomistic molecular dynamics simulations of H_2O diffusivity in liquid and supercritical CO_2

Othonas A. Moultos, Gustavo A. Orozco, Ioannis N. Tsimpanogiannis, Athanassios Z. Panagiotopoulos & Ioannis G. Economou

To cite this article: Othonas A. Moultos, Gustavo A. Orozco, Ioannis N. Tsimpanogiannis, Athanassios Z. Panagiotopoulos & Ioannis G. Economou (2015) Atomistic molecular dynamics simulations of H_2O diffusivity in liquid and supercritical CO_2 , Molecular Physics, 113:17-18, 2805-2814, DOI: 10.1080/00268976.2015.1023224

To link to this article: https://doi.org/10.1080/00268976.2015.1023224

Molecular Physics, 2015
Vol. 113, Nos. 17–18, 2805–2814, http://dx.doi.org/10.1080/00268976.2015.1023224

INVITED ARTICLE

Atomistic molecular dynamics simulations of H_2O diffusivity in liquid and supercritical CO_2

Othonas A. Moultos[a], Gustavo A. Orozco[b,†], Ioannis N. Tsimpanogiannis[a,c], Athanassios Z. Panagiotopoulos[b] and Ioannis G. Economou[a,*]

[a]*Chemical Engineering Program, Texas A&M University at Qatar, Doha, Qatar;* [b]*Department of Chemical and Biological Engineering, Princeton University, Princeton, United States;* [c]*Environmental Research Laboratory, Institute of Nuclear and Radiology Sciences and Technology, Energy and Safety, National Center for Scientific Research "Demokritos", Aghia Paraskevi, Greece*

(*Received 15 January 2015; accepted 18 February 2015*)

Molecular dynamics simulations were employed for the calculation of diffusion coefficients of pure CO_2 and of H_2O in CO_2 over a wide range of temperatures (298.15 K $< T <$ 523.15 K) and pressures (5.0 MPa $< P <$ 100.0 MPa), that are of interest to CO_2 capture-and-sequestration processes. Various combinations of existing fixed-point-charge force-fields for H_2O (TIP4P/2005 and Exponential-6) and CO_2 (elementary physical model 2 [EPM2], transferable potentials for phase equilibria [TraPPE], and Exponential-6) were tested. All force-field combinations qualitatively reproduce the trends of the experimental data for infinitely diluted H_2O in CO_2; however, TIP4P/2005–EPM2, TIP4P/2005–TraPPE and Exponential-6–Exponential-6 were found to be the most consistent. Additionally, for H_2O compositions ranging from infinite dilution to $x_{H_2O} = 0.36$, the Maxwell–Stefan diffusion coefficient is shown to have a weak non-linear composition dependence.

Keywords: diffusion coefficients; CO_2; H_2O; force-fields; molecular dynamics simulation

1. Introduction

In an effort to satisfy the ever-increasing global demand for energy consumption, large quantities of fossil fuels are currently utilised [1], which result in the production of significant amounts of CO_2 that are released in the atmosphere. The increase of the CO_2 concentration in the atmosphere has been identified as a major cause of the greenhouse gas effect and has a measurable effect on global climate. CO_2 capture and sequestration (CCS) has been suggested as a possible solution [2] to stabilise and later reduce CO_2 in the atmosphere.

A possible option for permanent CO_2 sequestration currently under consideration is the injection of the captured gas into geologic formations [3,4], such as producing or depleted gas/oil reservoirs [5,6], saline aquifers [7–9], and methane-gas-producing coal deposits or unmineable coal-seams [10,11]. During the initial stages of CO_2 injection in geologic formations, a CO_2-rich plume [12] is formed. Depending on the depth of injection, the plume can migrate towards (or away from) the surface, as a result of the density difference between the plume and the fluids in the surrounding formations. Of interest to the current study is aqueous-saturated formations. During the migration process, both CO_2 and H_2O mutually dissolve and subsequently diffuse in the other phase until thermodynamic equilibrium is reached.

The diffusivity of CO_2 in aqueous solutions and that of H_2O in liquid or supercritical CO_2 are two important transport parameters that are essential for the physical description and modelling of the process. Significant effort has been devoted to the experimental measurement and computational calculation of CO_2 diffusivity in aqueous solutions. Mutoru *et al*. [13] presented an extended collection (up to 2011) of experimental data for the diffusion coefficients of the binary system CO_2–H_2O and also reported a novel methodology for the calculation of the diffusion coefficient at infinite dilution of either of the two components. Additional recent experimental data were reported by Lu *et al*. [14] and Cadogan *et al*. [15]. A comprehensive review of computational studies was presented by Moultos *et al*. [16] who reported molecular dynamic (MD) calculations over a wide range of temperatures and pressures.

Although a large quantity of experimental data is available in the literature for the diffusion coefficient of CO_2 in H_2O (approximately 150 data points), relatively limited work has been reported on the diffusivity of H_2O in liquid or supercritical CO_2 (approximately 30 experimental data points). In particular, such data were reported by Xu *et al.* [17] at three different temperatures (i.e., 283, 298, and 308 K) and pressures in the range 130–300 bar, and Espinoza and Santamarina [18] at 296.5 ± 1.5 K and pressures in the range 78–144 bar. At these conditions, CO_2 is

*Corresponding author. Email: ioannis.economou@qatar.tamu.edu
†Current address: Physics Department, Universidad Antonio Nariño, Bogotá, Colombia

either liquid or supercritical. Schwertz and Brow [19] reported experimental data at 1 bar and temperatures in the range 307–352 K, for which CO_2 is in the vapour phase.

Molecular simulations of the phase equilibria of CO_2–H_2O mixtures have been reported by several groups [20–24]. Vlcek *et al*. [25] optimised the combination of SPC/E–EPM2 models (extended simple point charge [SPC/E]–transferable potentials for phase equilibria [TraPPE]), in the temperature range 298–348 K and pressure range 0.1–40.5 MPa in order to improve the predicted mutual solubility of CO_2 and H_2O. Subsequently, they used the improved models to obtain the mutual diffusivities. However, they reported relatively few calculated values for the diffusivity of H_2O in liquid or supercritical CO_2. Danten *et al*. [26] performed a limited number of MD simulations for the diffusivity of H_2O in CO_2 at near-critical ($T_r = 1.003$, where the subscript r denotes the reduced value of the temperature) or supercritical ($T_r = 1.26$) conditions. Recently, Orozco *et al*. [27] re-optimised the cross interaction parameters between CO_2 and H_2O molecules using fixed-point-charges force-fields, based on the Lennard-Jones and the Exponential-6 (Exp-6) functional forms, in order to improve the description of the mutual solubilities of the mixture. Specifically, the SPC/E–TraPPE (TraPPE, transferable potentials for phase equilibria) [28,29] combination was studied for the Lennard-Jones case, while for the Exp-6 case the H_2O and CO_2 models proposed by Errington and Panagiotopoulos [30] and Potoff *et al*. [31] were used, respectively. One of the main conclusions of the Orozco *et al.* study was that using the Lennard-Jones models, none of the examined combinations of unlike interaction parameters was able to represent adequately the properties of both phases. However, for the Exp-6 case, a re-optimisation of the interaction between unlike oxygen (i.e., oxygen of H_2O and oxygen of CO_2) was found to be sufficient for the prediction of the mutual solubilities of the H_2O-rich phase and of the CO_2-rich phase.

From the discussion up to this point, it is clear that a comprehensive evaluation of the various modern force-field combinations for H_2O and CO_2, with respect to their ability to predict the H_2O diffusivity, D_{H_2O}, over the range of temperatures and pressures relevant for CCS operations is still lacking. This is the main focus of the present study. In particular, we report an extensive series of MD simulations for a wide range of temperatures (298.15–523.15 K) and pressures (5.0–100.0 MPa), and for various combinations of force fields. Initially, we examine H_2O in CO_2 at infinite dilution (i.e., for temperatures up to 423.15 K). Subsequently, we examine the case of higher temperatures (i.e., 473.15 and 523.15 K) where the solubility of H_2O in CO_2 can be significantly higher (up to mole fraction of approximately 0.36).

The paper is organised as follows. In Section 2, we present the intermolecular potentials and simulation methods that we use. Section 3 refers to our MD simulation results and their discussion, which generally are in good agreement with reported experimental data. The reported results clearly indicate that the diffusivity of H_2O in CO_2 depends on both pressure and temperature while a weak composition dependence is identified. Finally, we end with the conclusions.

2. Models and methods

2.1. Intermolecular potentials

The TIP4P/2005 [32] and Exp-6 [30] force-fields were used for the representation of H_2O molecules, while the EPM2 [33], TraPPE [29], Exp-6 [31], and two optimised models proposed by Zhang and Duan (ZD) [34] and Merker *et al*. [35] were employed for CO_2. The TIP4P/2005 [32] is a rigid 4-site model in which a Lennard–Jones (LJ) sphere is fixed on the oxygen site. The electrostatic contributions are implemented by positive partial charges located on each hydrogen atom and a negative partial charge fixed on an 'M-site', located on the bisector of the H–O–H angle at 0.1546 Å from the oxygen atom. All the CO_2 force-fields used are rigid linear 3-site models, with partial charges fixed on the axis of symmetry of the molecules. Negative partial charges are located on the oxygen atoms and positive ones on the carbon LJ sites, with an exception of the model proposed by Merker *et al.* [35] for which the positive partial charges are located on the molecular axis at a distance $l_{Cq} = \pm 0.2$ Å from the oxygen atom. The original force-field proposed by Merker *et al.* [35] has a point quadrupole rather than point-charges, but the authors developed an additional point-charge model for easier computational implementation in commonly used molecular simulation codes, which is used here.

The total interactions between molecules i and j, with a total number of m and n sites, respectively, were calculated as the sum of LJ repulsion-dispersion interactions and the Coulomb interactions:

$$U_{ij}^{LJ} = \sum_{a=1}^{m}\sum_{b=1}^{n}\left(4\varepsilon_{ij}^{ab}\left[\left(\frac{\sigma_{ij}^{ab}}{r_{ij}^{ab}}\right)^{12} - \left(\frac{\sigma_{ij}^{ab}}{r_{ij}^{ab}}\right)^{6}\right] + \frac{q_i^a q_j^b}{4\pi\varepsilon_0 r_{ij}^{ab}}\right) \tag{1}$$

where ε_{ij}^{ab} and σ_{ij}^{ab} are the LJ interaction parameters between site a in molecule i and site b in molecule j, respectively, r_{ij}^{ab} is the distance between sites a and b, q_i^a and q_j^b are the charges on site a and b respectively, and ε_0 is the dielectric constant in vacuum.

The Exp-6 (Buckingham-type [36]) models used are also fixed-point-charge force-fields, with the site–site interactions given by the following expression:

$$U_{ij}^{\exp-6} = \sum_{a=1}^{m}\sum_{b=1}^{n}\left(\frac{\varepsilon_{ij}^{ab}}{1-\frac{6}{a_{ij}^{ab}}}\left[\frac{6}{a_{ij}^{ab}}\exp\left(a_{ij}^{ab}\left[1-\frac{r_{ij}^{ab}}{r_{m,ij}^{ab}}\right]\right) - \left(\frac{r_{m,ij}^{ab}}{r_{ij}^{ab}}\right)^{6}\right] + \frac{q_i^a q_j^b}{4\pi\varepsilon_0 r_{ij}^{ab}}\right) \tag{2}$$

Table 1. Force-field parameters for H_2O and CO_2 examined in this study.

H_2O			CO_2					
	TIP4P/2005 [32]	Exp-6 [27]		EPM2 [33]	TraPPE [29]	ZD [34]	Merker *et al.* [35]	Exp-6 [27]
H–O–H (°)	104.52	109.47	O–C–O (°)	180	180	180	180	180
$l_{O\text{-}H}$ (Å)	0.9572	1.0668	$l_{O\text{-}C}$ (Å)	1.149	1.16	1.163	1.2869	1.1433
σ_O (Å)	3.1589	3.1947	l_{Cq}(Å)	0	0	0	0.2	0
σ_H (Å)	0	0	σ_C (Å)	2.757	2.8	2.7918	2.8137	2.753
ε_O/k_B (K)	93.2	159.78	σ_O (Å)	3.033	3.05	3.0	2.9755	3.029
ε_H/k_B (K)	0	0	ε_C/k_B (K)	28.129	27	28.845	12.3724	29.07
q_O (e)	−1.1128	−0.7374	ε_O/k_B (K)	80.507	79	82.656	100.493	83.2
q_H (e)	0.5564	0.3687	q_C (e)	0.6512	0.7	0.5888	21.2	0.6466
a_O	–	12	q_O (e)	−0.3256	−0.35	−0.2944	−10.6	−0.3233
a_H	–	0	a_C	–	–	–	–	14
$\varepsilon_{O(CO2)\text{-}O(H2O)}/k_B$ (K)		105.29	a_O	–	–	–	–	14

where ε_{ij}^{ab}, a_{ij}^{ab} and $r_{m,ij}^{ab}$ are the Exp-6 parameters. The values for all the potential parameters used in the current study are listed in Table 1.

The LJ parameters for the interaction between atoms belonging to different molecules were calculated using the Lorentz–Berthelot combining rules [37]. An exception was made for the EPM2 model, for which the distance σ_{ij}^{ab} between unlike sites of CO_2 molecules was given by the geometric mean, in accordance with the original work [33]. Consequently, cross-interaction parameters were calculated from the expressions,

$$\varepsilon_{ij}^{ab} = \left(\varepsilon_i^a \varepsilon_j^b\right)^{\frac{1}{2}} \tag{3}$$

$$\sigma_{ij}^{ab} = \begin{cases} \left(\sigma_i^a \sigma_j^b\right)^{\frac{1}{2}} & \text{for } a, b = C_{CO_2}, O_{CO_2} \\ & \text{for the EPM2 model} \\ \frac{1}{2}\left(\sigma_i^a + \sigma_j^b\right) & \text{otherwise} \end{cases} \tag{4}$$

For the Exp-6 model, in nearly all cases the combining rules correspond to the geometric-mean or ε_{ij}^{ab} and a_{ij}^{ab} and the arithmetic-mean for $r_{m,ij}^{ab}$. The expressions are the following (ε_{ij}^{ab} is shown in Equation (3)):

$$a_{ij}^{ab} = \left(a_i^a a_j^b\right)^{\frac{1}{2}} \tag{5}$$

$$r_{m,ij}^{ab} = \frac{1}{2}\left(r_{m,i}^a + r_{m,j}^b\right) \tag{6}$$

The only exception to these combining rules is for the unlike interaction parameter ε_{ij}, between the oxygen of H_2O and the oxygen of CO_2. As already mentioned, it has been recently re-optimised by Orozco *et al.* [27] in order to improve the mutual solubility predictions of the binary mixture CO_2–H_2O. The optimised value for this parameter is also listed in Table 1.

2.2. Computational details

In this work, all MD simulations were performed in the isothermal-isobaric (NPT) ensemble, in a cubic box with periodic boundary conditions imposed in all directions. A majority of simulations presented in this paper correspond to systems with 1000 CO_2 molecules. The system was initially allowed to equilibrate for a period of 5 ns with integration timestep of 1 fs, using a Berendsen thermostat and barostat [38], with coupling constants for both set to 1 ps. During this period, the density of the system converged to a mean value, corresponding to the temperature and pressure conditions set. Subsequently, 10 ns production runs were performed, again with integration timestep of 1 fs. The temperature and pressure were maintained constant using the Berendsen method with the coupling constant of the thermostat set to 0.2 ps and of the barostat to 1 ps. Monitoring of energy, pressure, and temperature during the production period showed that they were well stabilised, with small fluctuations present (less than 1% for energy and temperature and less than 15% for pressure), typical for any MD simulation. The molecular trajectories were sampled every 10,000 steps, resulting in a total of 1000 configurations per simulation, from which all properties of interest were calculated.

Long-range Coulombic interactions were handled using the particle mesh Ewald (PME) method [39,40], which does not directly sum the wave vectors but assigns the charges to a grid using cardinal *B*-spline interpolation and thus exhibits a faster scaling than the ordinary Ewald summation method [41]. In all the simulations performed, a fourth-order (cubic) interpolation was used along with a Fourier-spacing parameter of 0.12, corresponding to an accuracy approximately 5×10^{-3} in electrostatic energy calculations. The cut-off distance was set to 12 Å, both for the LJ interactions and the PME.

All the simulations were executed with the open-source package GROMACS [42,43] (version 4.6.3), which is

generally acknowledged to be a highly optimised and efficient MD simulator [44,45]. Each run was executed in 16–32 cores, with Intel Xeon 2.7 GHz processors, and needed about 1–4 wall-clock hours to be completed.

For the case of infinite diluted H_2O in CO_2, the diffusion coefficients were calculated using the Einstein relation, according to which the self-diffusion coefficient is obtained from the solute mean square displacement, [46]

$$D_{H_2O}^{self} = \frac{1}{6} \lim_{t\to\infty} \frac{d}{dt} \left\langle \frac{1}{N} \sum_{i=1}^{N_{H_2O}} [r_i(0) - r_i(t)]^2 \right\rangle \quad (7)$$

where $r_i(t)$ is the unfolded positions of the centres of mass of H_2O molecules at time t, and the angle brackets indicate an ensemble average over all molecules and time origins. In order to improve the statistics of our results, the diffusion coefficient for each state point was calculated from 20 different simulations, each one starting from a completely different initial configuration, thus leading to a wide divergence of the trajectories of the molecules. We obtained the final results of diffusivities by averaging the diffusion coefficients from the individual runs.

For the case of higher H_2O compositions up to $x_{H_2O} = 0.36$, the Maxwell–Stefan diffusion coefficient of H_2O in CO_2 was calculated according to [47]

$$D_{MS} = \frac{1}{6N x_{H_2O}\, x_{CO_2}} \left(\frac{m_{H_2O}}{m_{CO_2}} x_{H_2O} + x_{CO_2} \right)^2 \times \lim_{t\to\infty} \frac{d}{dt} \left\langle \left[\sum_{i=1}^{N_{H_2O}} r_i(0) - \sum_{i=1}^{N_{H_2O}} r_i(t) \right]^2 \right\rangle \quad (8)$$

where N is the total number of molecules, x_{H_2O} and x_{CO_2} are the mole fractions, m_{H_2O} and m_{CO_2} are the molecular masses of H_2O and CO_2, respectively, and $r_i(t)$ is the unfolded position of H_2O molecule i at time t. The angle brackets indicate an ensemble average over all time origins.

2.3. *System-size dependence of diffusion coefficient*

It has been previously reported in the literature that system size effects in the calculation of transport properties of pure fluids should be taken into account [48–50]. Consequently, a systematic analysis of system size effects was performed both for the pure CO_2 and H_2O in CO_2 diffusion coefficient. For the case of pure CO_2, MD simulations for systems with 250, 1000, and 4000 CO_2 molecules were performed and results were found to vary linearly with the inverse of the box length, $1/L$. Consequently, the linear correlation was extrapolated to infinite system size in order to estimate the diffusion coefficient at the thermodynamic limit. In the Supplemental data section (Tables S1–S5), MD simulations for the systems with 1000 molecules and the extrapolated infinite size value are reported. Simulations revealed that the system size effect becomes stronger at higher temperatures and lower densities. Representative results are shown in Figure S1 of Supplemental Information. At 283.15 K and 20 MPa the diffusion coefficient of pure CO_2 increases by 9.8% when the simulation box increases from 250 to 4000 molecules whereas at 323.15 K the increase is 15% (Figure S1(a) in Supplemental data section). At 523.15 K, the increase in self-diffusivity is approximately 80% and 181% for 50 MPa and 10 MPa, respectively (Figure S1(b) in Supplemental data section).

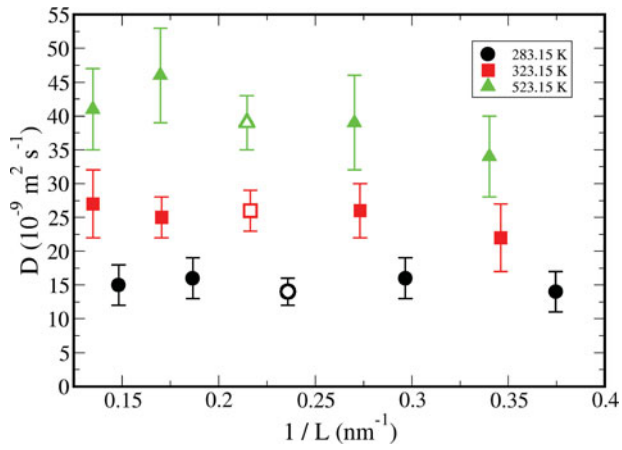

Figure 1. Infinite dilution diffusion coefficient of H_2O in CO_2 at 283.15 and 323.15 K (20 MPa), and 523.15 K (100 MPa) from MD simulations. The force-fields used are TIP4P/2005 for H_2O and EPM2 for CO_2. Open symbols correspond to 1000 CO_2 molecules which is the standard system size used for obtaining the results in Figures 2–5.

For the case of H_2O in CO_2 at infinite dilution, 1 H_2O molecule was dissolved in CO_2, while for the case of higher H_2O compositions the number of molecules used was calculated accordingly. In order to address the magnitude of system size effects for the case of mixtures, a thorough investigation was made by varying the number of CO_2 molecules (solvent) in the system. In Figure 1, the diffusion coefficient of 1 TIP4P/2005 H_2O molecule in 250, 500, 1000, 2000, and 4000 EPM2 CO_2 molecules are presented at 283.15 K (20 MPa), 323.15 K (20 MPa), and 523.15 K (100 MPa). From Figure 1, one can see that the diffusion coefficient of H_2O in CO_2 remains practically constant, within the statistical error, for the different box lengths examined. For the larger systems studied (greater than 1000 solvent molecules), the computational time required for the simulation is more than five times higher and thus large systems are not considered computationally efficient.

3. Results and discussion

3.1. *CO_2 self-diffusion coefficient*

The accuracy of various force-fields in predicting the self-diffusion coefficient of pure CO_2 was initially examined. All results presented in this section and in Figure 2

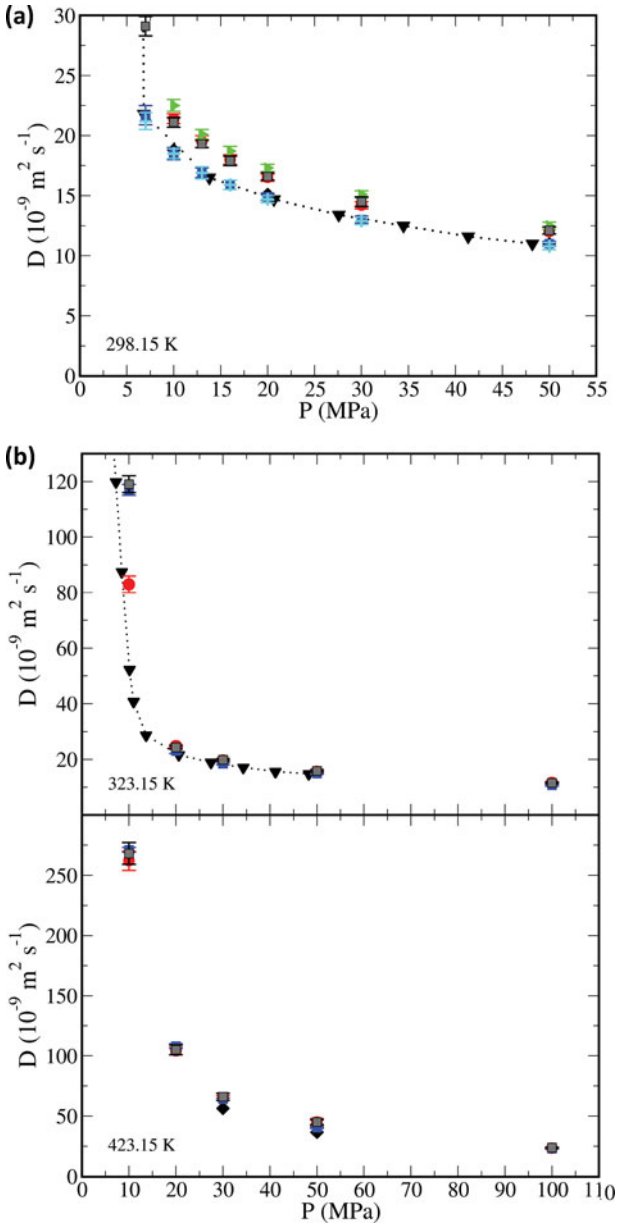

Figure 2. Self-diffusion coefficient of CO_2 as a function of pressure at (a) 298.15 K and (b) 323.15 K (top) and 423.15 K (bottom). Experimental data from Ref. [51] (black inverse triangles) and Ref. [52] (black diamonds). MD simulation results using the following models: EPM2 (red circles); TraPPE (blue squares); ZD [34] (green right triangles); Merker *et al.* [35] (cyan crosses); Exp-6 (black dashed squares). The dotted line, connecting the experimental values, is drawn to guide the eye.

refer to the infinite-system extrapolated values of pure CO_2 self-diffusivities, according to the system-size dependence discussed in detail previously. Experimental measurements of the CO_2 self-diffusion coefficient are available in the literature [51,52] for a wide range of temperatures and pressures and thus a useful comparison with MD simulations can be made. As mentioned earlier, five force-fields were considered in this study for the representation of CO_2 molecules.

In Figure 2(a), the self-diffusion coefficient of CO_2 at 298.15 K is shown as a function of pressure (up to 50 MPa), using the experimental measurements reported by Etesse *et al.* [51] and Groβ *et al.* [52] and the simulations performed in this study. As the pressure decreases approaching the critical pressure of 7.4 MPa, the self-diffusion coefficient increases, although temperature is below the critical value of 304.12 K. All the models tested follow qualitatively the experimental trend; however, TraPPE and the force-field by Merker *et al.* [35] are more accurate at all pressures, exhibiting almost identical results with each other and an excellent agreement with the experimental data. More specifically, the self-diffusion coefficients predicted by the TraPPE model show absolute deviations from the experimental data in the range of 0%–2.4%, while predictions for the Merker *et al.* [35] model from 0%–2.8%. All the other models clearly overestimate the diffusion coefficients by 9%–33%, with the ZD [34] model being the most inaccurate in the entire pressure range, deviating from the experimental measurements by an average absolute deviation of 18%.

The latter result is in contrast with the recent simulation study by Aimoli *et al.* [53], in which the authors concluded that the ZD model provides the most accurate self-diffusion coefficient, in the temperature and pressure range studied. The primary reason for this difference is the system-size-dependence correction applied in the present study, as discussed in detail in the previous section. Aimoli *et al.* [53] used 1000 CO_2 molecules for all their simulations, in order to mitigate any size dependencies. In this work, MD simulations are compared to calculations reported by Aimoli *et al.* [53] In Figure S2 of Supplemental Information document, a direct comparison of the self-diffusion coefficients of the EPM2, TraPPE, and ZD models and experimental data at 298.15 K is shown. Our calculations with 1000 molecules are in excellent agreement with the ones by Aimoli *et al*. [53] for all three models. At the same time, application of the system size correction reveals that the ZD model is the least accurate of the three.

In Figure 2(b), the self-diffusion coefficients of CO_2 are shown at two supercritical temperatures at 323.15 (top) and 423.15 K (bottom) as a function of pressure. At 323.15 K, there is a sharp increase of D_{CO_2} as pressure decreases below 10 MPa, typical of a supercritical fluid. At 5 MPa, D_{CO_2} decreases by approximately a factor of 3 from 298.15 to 323.15 K and by another factor of 2 at 423.15 K. At these two high temperatures, MD simulations of the EPM2, TraPPE, and Exp-6 models are shown only. For pressures higher than 20 MPa all three model predictions are in very good agreement with experimental data. For the low pressure simulated at 323.15 K (10 MPa) no model was able to accurately predict the self-diffusion coefficient of CO_2. All three models tested over-predict diffusivity by 60%–129%, a fact that can be partially explained by their inability to

accurately estimate the CO_2 density at these near critical conditions [54]. In the Supplemental Information section, we provide MD simulation results for the self-diffusion coefficients of CO_2 over a broad range of conditions, including temperatures and pressures not measured experimentally.

3.2. *Diffusion coefficient of H_2O in CO_2 at infinite dilution*

Atomistic NPT simulations were performed for various combinations of TIP4P/2005 H_2O model with various CO_2 force-fields. TIP4P/2005 is one of the most recent force-fields for H_2O [32] and it provides a very accurate prediction both for H_2O self-diffusion coefficient [55] and CO_2 diffusivity in H_2O [16]. Therefore, it is expected to provide adequately accurate predictions for the H_2O diffusion coefficient in CO_2. The present study is done at temperatures ranging from 283.15 to 523.15 K and pressures from 5 to 100 MPa. These conditions correspond to liquid and supercritical CO_2. Xu *et al.* [17] have reported experimental nuclear magnetic resonance (NMR) measurements of the diffusivity of H_2O in CO_2 for 283.15, 298.15, and 308.15 K and for pressures from approximately 13 to 30 MPa.

In Figure 3, the MD simulation results are presented and compared to experimental data by Xu *et al.* [17] All force-field combinations follow the trend of the experimental data and show a decrease in diffusivity with the increase of pressure, but with variable accuracy. Specifically, at 283.15 K (Figure 3 top), the Exp-6 models and the TIP4P/2005–TraPPE combination follow the experiments very accurately. The Exp-6 models deviate from the experimental values by approximately 3%–4%, while the TIP4P/2005–TraPPE combination gives slightly overestimated values. The combination of TIP4P/2005 with the model proposed by Merker *et al.* [35] gives estimates very closely related to the case of TIP4P/2005–TraPPE. MD simulations using EPM2 and the ZD [34] force-field predict overestimated diffusivities, with the latter one being the most inaccurate exhibiting 35%–45% deviation from experimental data for the pressure range examined.

At 298.15 K, all combinations of models show better accuracy than at 283.15 K, with deviations from experimental values ranging between 0% and 10%, except for the combination TIP4P/2005–ZD, which overestimates the diffusion coefficients by approximately 25%.

The near-critical behaviour of the solvent results in a sharp increase of the diffusion coefficient at the highest temperature shown (308.15 K) and pressures below 10 MPa. At this temperature, the combination containing the EPM2 model is clearly the most accurate followed closely by the combination of TIP4P/2005–ZD. The rest of the model combinations underestimate the diffusion coefficient of H_2O in CO_2 by up to 25%.

It should be pointed out that all simulated values are close to the self-diffusion coefficients of CO_2 at the same temperature and pressure, presented in the previous section, indicating that diffusivity is primarily driven by the free volume of the system. In Figure 4, experimental data [54] and MD calculations for the density of pure CO_2 are presented. As can be seen, all models are in good agreement with the experimental values, with the Exp-6 and TraPPE models being the most accurate. The percentage average deviation from experimental data is less than 1.8% at the conditions

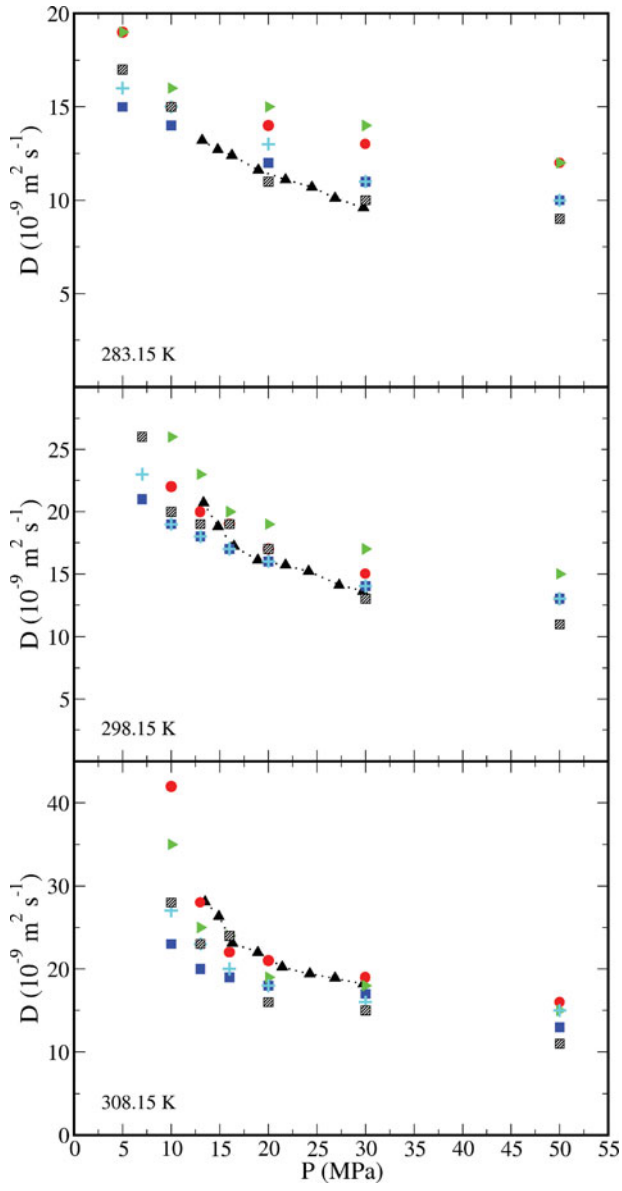

Figure 3. Infinite dilution diffusion coefficient of H_2O in CO_2 as a function of pressure at 283.15 K (top), 298.15 K (middle), and 308.15 K (bottom). Experimental data from Ref. [17] (black triangles). All other symbols are the same as in Figure 2 (TIP4P/2005 H_2O model is used for all combinations except for the one with Exp-6). Error bars are excluded for clarity. The statistical uncertainty is 2–3 times the symbol size. The dotted line, connecting the experimental values, is drawn to guide the eye.

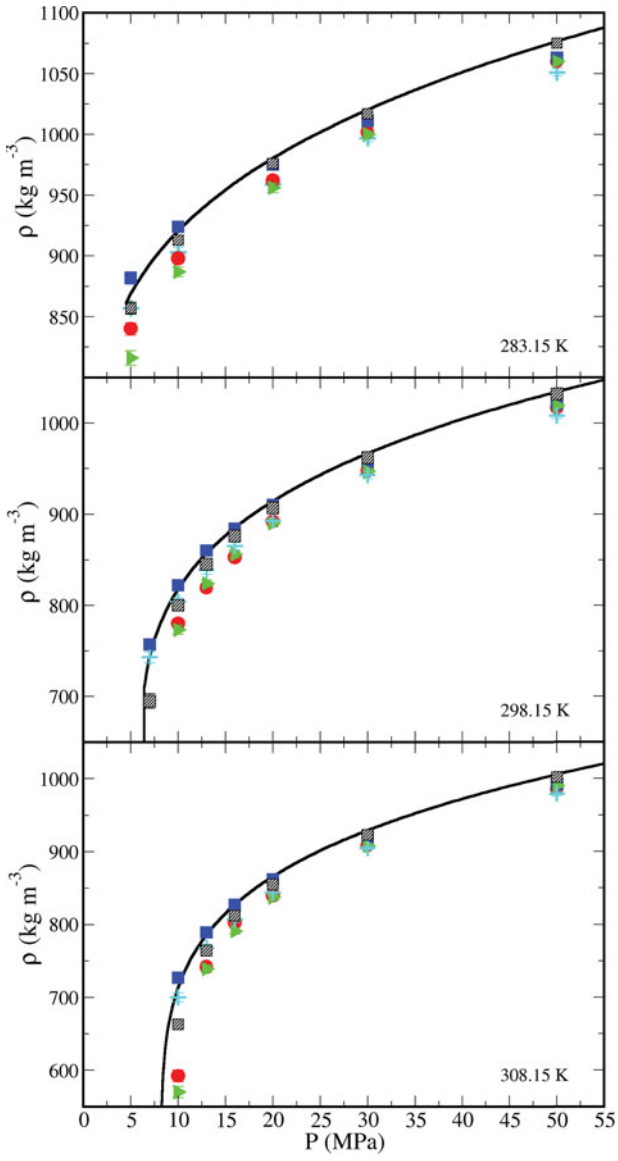

Figure 4. Density of CO_2 as a function of pressure at 283.15 K (top), 298.15 K (middle), and 308.15 K (bottom). All symbols are the same as in Figure 2. The black line shows the experimental values from National Institute of Standards and Technology (NIST) database [54].

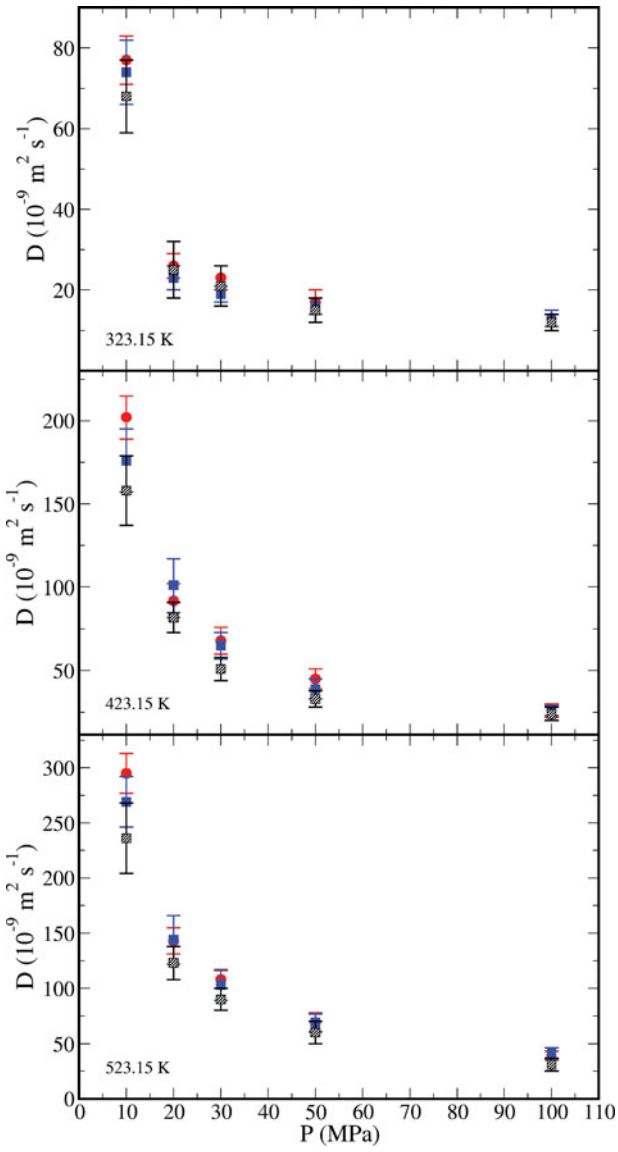

Figure 5. Infinite dilution diffusion coefficient of H_2O in CO_2 as a function of pressure at 323.15 K (top), 423.15 K (middle), and 523.15 K (bottom). All symbols are the same as in Figure 2.

examined. This is in line with their accuracy in the prediction of diffusivities at 283.15 and 298.15 K. Predictions for the CO_2 density were compared to recent calculations by Aimoli *et al.* [56] for the same force-fields. Representative results from 250 to 550 K at 10 and 100 MPa are shown in Figure S3. Excellent agreement between the two sets of calculations and with experimental data is observed in all cases.

MD simulations were also performed at higher temperatures. In Figure 5, the infinite dilution diffusion coefficient of H_2O in CO_2 in the range 323.15–523.15 K as a function of pressure is shown. For these conditions, no experimental or calculated values are available for comparison. Given the accuracy of the models at lower temperatures, one can consider these data as accurate predictions of the actual values. For these particular calculations, we used the combinations of TIP4P/2005 with EPM2 and TraPPE force-fields and the Exp-6–Exp-6, since the remaining combinations were either less or equally accurate with the selected ones. Again, the diffusivity decreases with the increase of pressure (and density) and the various combinations of models predict approximately the same diffusivity values, with the combination containing EPM2 model resulting in slightly higher values. This can be partially explained by the fact that all the models give very similar density predictions.

3.3. Diffusion coefficient of H_2O in CO_2 at higher concentrations

We performed simulations of the H_2O diffusion coefficient in CO_2 at 473.15 and 523.15 K, for 10, 20, and 100 MPa and for concentrations ranging from infinite dilution up to the solubility limit, as reported by Liu *et al.* [23] and Orozco *et al.* [27] for each combination of models. Since the solubility of H_2O in the CO_2 phase is substantial, we calculated the Maxwell–Stefan diffusion coefficient (Equation (8)). Based on the accuracy discussed above, the combinations of force-fields used here were TIP4P/2005–TraPPE and Exp-6–Exp-6. These two combinations of models deviate from each other for the solubility of H_2O in CO_2 [23,27]. More specifically, at 473.15 K the TIP4P/2005–TraPPE combination predicts that the H_2O solubility in CO_2 is almost constant and approximately equal to 0.1 for the entire pressure range, while the combination of Exp-6 models gives a value of approximately 0.15. For the higher temperature of 523.15 K, the solubility of H_2O in CO_2, for the combination of TIP4P/2005–TraPPE was shown to be approximately 0.2, 0.13, and 0.18 for 10, 20, and 100 MPa, respectively. The combination of Exp-6 force-fields yields higher values of solubility ranging from approximately 0.3 to 0.35, depending on pressure.

In Figure 6, the MD predictions for Maxwell–Stefan diffusion coefficients (D_{MS}) of H_2O in CO_2 at 473.15 K for the three pressures examined (10, 20, and 100 MPa) and the two combinations of models are shown. For the lowest pressure examined at 10 MPa (Figure 6 top), D_{MS} from both sets of force-fields increases with the H_2O mole fraction. The increase is more pronounced for the case of Exp-6 models, which also give higher values of D_{MS} for the entire range of mole fractions. At 20 MPa, again the Exp-6 models give higher values of D_{MS} diffusivity in comparison with TIP4P/2005–TraPPE combination. For this specific pressure, the D_{MS} diffusion coefficient of H_2O in CO_2 at infinite dilution is lower than the one obtained for the H_2O mole fraction of approximately 0.05, but a further increase in H_2O mole fraction does not have an effect, within the statistical uncertainty of the calculations. For the highest pressure studied (100 MPa, Figure 6 bottom), D_{MS} from TIP4P/2005–TraPPE increases with H_2O composition; however, the Exp-6–Exp-6 combination, that covers a broader range of compositions, predicts that D_{MS} goes through a maximum and then decreases.

As shown in Tables 6 and 7 of the Supplemental data section, both the TraPPE and Exp-6 models give very similar density estimations, for the whole range of conditions studied, and therefore their differences, as described above, can only be attributed to the H_2O–CO_2 cross interactions.

In Figure 7, the MD simulation results for Maxwell–Stefan diffusion coefficients (D_{MS}) of H_2O in CO_2 at 523.15 K for the pressure range 10–100 MPa and the two models are presented. For this temperature, the solubility of H_2O in CO_2 is raised up to approximately 0.35 for the high pressures examined (20 and 100 MPa) and more than 0.3 for 10 MPa for the Exp-6 models combination. For the latter pressure, the D_{MS} remains constant for H_2O mole fractions greater than 0.05. At 100 MPa, D_{MS} exhibits a similar behaviour to 473 K and 100 MPa, going through a maximum at low H_2O composition and then decreases. For this pressure (100 MPa), the two combinations of models show an improved agreement to each other.

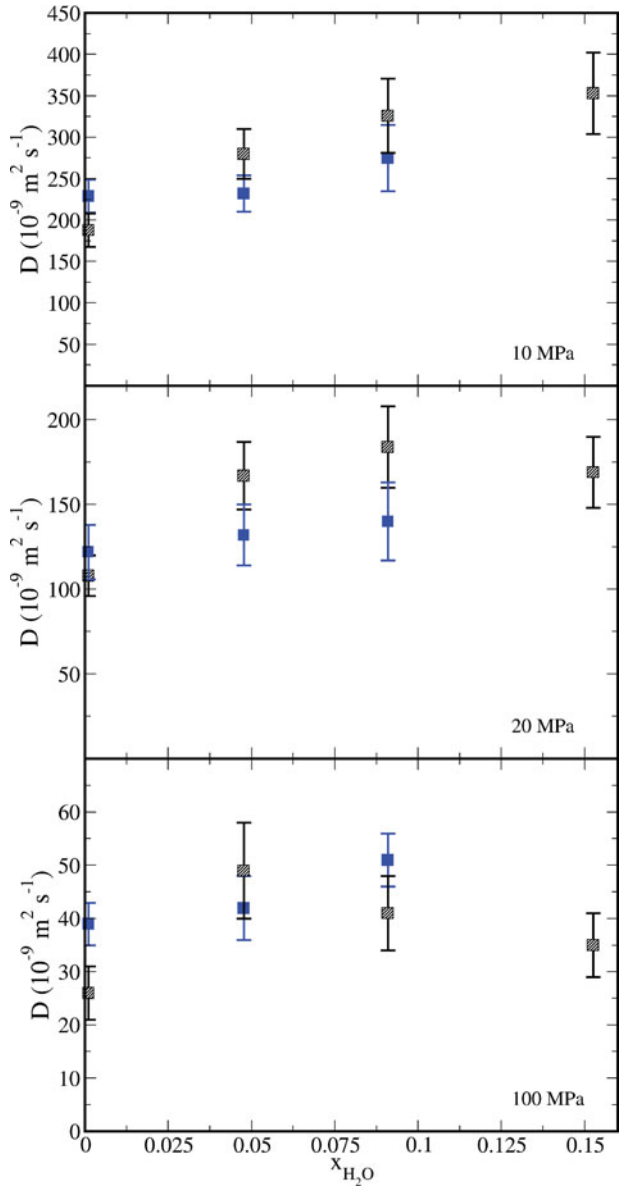

Figure 6. Maxwell–Stefan diffusion coefficient (D_{MS}) of H_2O in CO_2 as a function of H_2O mole fraction at 473.15 K and 10, 20, and 100 MPa. Blue and black dashed squares refer to D_{MS} for TIP4P/2005–TraPPE and Exp-6–Exp-6 combinations respectively.

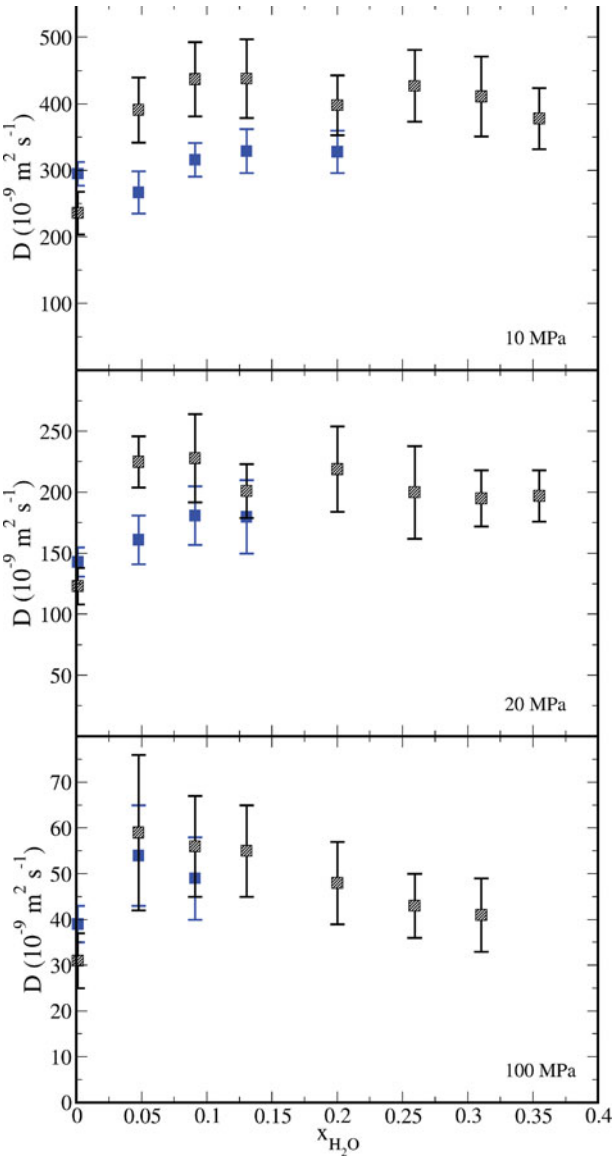

Figure 7. Maxwell–Stefan diffusion coefficient (D_{MS}) of H_2O in CO_2 as a function of H_2O mole fraction for 523.15 K and 10, 20, and 100 MPa. The symbols are the same as in Figure 6.

4. Conclusions

In this study, we presented a series of MD simulations for the calculation of diffusion coefficients of pure CO_2 and of H_2O in CO_2 over a wide range of temperatures (298.15 K $< T <$ 523.15 K) and pressures (5.0 MPa $< P <$ 100.0 MPa). Various combinations of force-fields for H_2O with CO_2 (TIP4P/2005 with EPM2, TraPPE, ZD, Merker *et al.* and Exp-6–Exp-6) were evaluated. The MD results were in very good agreement with the available experimental data at infinite dilution. Overall, the combinations TIP4P/2005–EPM2, TIP4P/2005–TraPPE and Exp-6–Exp-6 with optimised cross interactions between oxygen atoms from unlike molecules were found to be the most accurate for the temperature and pressure ranges examined.

Maxwell–Stefan diffusion coefficient of H_2O in CO_2 is also examined for compositions up to 0.36, at 473.15 K and 523.15 K and pressures up to 100 MPa. Maxwell–Stefan diffusion coefficient was shown to have a weak non-linear dependence on composition. No experimental data are available for these concentrations and thus no definite conclusions concerning the accuracy of force-fields can be made.

The results from the current study, in combination with the recent calculations of diffusivity in H_2O [16] and the phase equilibria studies by Liu *et al.* [23] and Orozco *et al.* [27] provide a thorough evaluation of the most accurate and widely used CO_2 and H_2O force-fields in their ability to predict thermodynamic and transport properties. In order for a more concrete conclusion to be drawn regarding the accuracy of the various force-fields, additional experimental work is needed at high H_2O compositions and calculations for other transport properties (such as viscosity, thermal conductivity, and surface tension).

Finally, a significant system size effect was found for the self-diffusion coefficient of pure CO_2. This effect was accounted by performing simulations at different system sizes and extrapolating calculations to the thermodynamic limit. In the future, a more systematic analysis will be performed.

Acknowledgements

This publication was made possible by NPRP [grant number 6-1157-2-471] form the Qatar National Research Fund (a member of Qatar Foundation). The statements made herein are solely the responsibility of the authors. We are grateful to the High Performance Computing Center of Texas A&M University at Qatar for generous resource allocation.

Disclosure statement

No potential conflict of interest was reported by the authors.

Funding

NPRP [grant number 6-1157-2-471] form the Qatar National Research Fund (a member of Qatar Foundation).

Supplemental data

Supplemental data for this article can be accessed at http://dx.doi.org/10.1080/00268976.2015.1023224.

References

[1] International Energy Agency. *World Outlook* (IEA, Paris, 2006).

[2] B. Metz, O. Davidson, H. de Concinck, M. Loos, and L. Meyer, *Carbon Dioxide Capture and Storage: Special Report of the Intergovernmental Panel on Climate Change* (Cambridge University Press, Cambridge, UK, 2005).

[3] R.S. Middleton, G.N. Keating, P.H. Stauffer, A.B. Jordan, H.S Viswanathan, Q.J. Kang, J.W. Carey, M.L. Mulkey, E.J. Sullivan, S.P. Chu, R. Esposito, and T.A. Meckel, Energy Environ. Sci. **5**, 7328 (2012).
[4] Q. Schiermeier, Nature **442**, 620 (2006).
[5] C.M. Oldenburg, K. Pruess, and S.M. Benson, Energy & Fuels **15**, 293 (2001).
[6] A.R. Kovscek, Pet. Sci. Technol. **20**, 841 (2002).
[7] S. Bachu and J.J. Adams, Energy Convers. Manag. **44**, 3151 (2003).
[8] K. Michael, A. Golab, V. Shulakova, J. Ennis-King, G. Allinson, S. Sharma, and T. Aiken, Int. J. Greenh. Gas Con. **4**, 659 (2010).
[9] M. Steele-MacInnis, R.M. Capobianco, R. Dilmore, A. Goodman, G. Guthrie, J.D. Rimstidt, and R.J. Bodnar, Environ. Sci. Tech. **47**, 79 (2013).
[10] J. Gale and P. Freund, Environ. Geosci. **8**, 210 (2001).
[11] S. Mazumder, P. van Hemert, J. Bruining, K.-H.A.A. Wolf, and K. Drabe, Fuel **85**, 1904 (2006).
[12] S.J. Altman, B. Aminzadeh, M.T. Balhoff, P.C. Bennett, S.L. Bryant, M.B. Cardenas, K. Chaudhary, R.T. Cygan, W. Deng, T. Dewers, D.A. DiCarlo, P. Eichhubl, M.A. Hesse, C. Huh, E.N. Matteo, Y. Mehmani, C.M. Tenney, and H. Yoon, J. Phys. Chem. C **118**, 15103 (2014).
[13] J.W. Mutoru, A. Leahy-Dios, and A. Firoozabadi, AIChE J. **57**, 1617 (2011).
[14] W. Lu, H. Guo, I.M. Chou, R.C. Burruss, and L. Li, Geochim. Cosmochim. Acta **115**, 183 (2013).
[15] S.P. Cadogan, G.C. Maitland, and J.P.M. Trusler, J. Chem. Eng. Data **59**, 519 (2014).
[16] O.A. Moultos, I.N. Tsimpanogiannis, A.Z. Panagiotopoulos, and I.G. Economou, J. Phys. Chem. B **118**, 5532 (2014).
[17] B. Xu, K. Nagashima, J.M. DeSimone, and C.S. Johnson, J. Phys. Chem. A **107**, 1 (2002).
[18] D.N. Espinoza and J.C. Santamarina, Water Resour. Res. **46**, W07537 (07531–07510) (2010).
[19] F.A. Schwertz and J.E. Brow, J. Chem. Phys. **19**, 640 (1951).
[20] J. Vorholz, V.I. Harismiadis, B. Rumpf, A.Z. Panagiotopoulos, and G. Maurer, Fluid Phase Equilib. **170**, 203 (2000).
[21] J. Vorholz, V.I. Harismiadis, A.Z. Panagiotopoulos, B. Rumpf, and G. Maurer, Fluid Phase Equilib. **226**, 237 (2004).
[22] M. Lisal, W.R. Smith, and K. Aim, Fluid Phase Equilib. **228**, 345 (2005).
[23] Y. Liu, A.Z. Panagiotopoulos, and P.G. Debenedetti, J. Phys. Chem. B **115**, 6629 (2011).
[24] Y. Liu, T. Lafitte, A.Z. Panagiotopoulos, and P.G. Debenedetti, AIChE J. **59**, 3514 (2013).
[25] L. Vlcek, A.A. Chialvo, and D.R. Cole, J. Phys. Chem. B **115**, 8775 (2011).
[26] Y. Danten, T. Tassaing, and M. Besnard, J. Chem. Phys. **123**, 074505 (2005).
[27] G.A. Orozco, I.G. Economou, and A.Z. Panagiotopoulos, J. Phys. Chem. B 11504 (2014).
[28] H.J.C. Berendsen, J.R. Grigera, and T.P. Straatsma, J. Phys. Chem. **91**, 6269 (1987).
[29] J.J. Potoff and J.I. Siepmann, AIChE J. **47**, 1676 (2001).
[30] J.R. Errington and A.Z. Panagiotopoulos, J. Phys. Chem. B **102**, 7470 (1998).
[31] J.J. Potoff, J.R. Errington, and A.Z. Panagiotopoulos, Mol. Phys. **97**, 1073 (1999).
[32] J.L.F. Abascal and C. Vega, J. Chem. Phys. **123**, 234505 (2005).
[33] J.G. Harris and K.H. Yung, J. Phys. Chem. **99**, 12021 (1995).
[34] Z. Zhang and Z. Duan, J. Chem. Phys. **122**, 214507 (2005).
[35] T. Merker, C. Engin, J. Vrabec, and H. Hasse, J. Chem. Phys. **132**, 234512 (2010).
[36] G.A. Orozco, O.A. Moultos, H. Jiang, I.G. Economou, and A.Z. Panagiotopoulos, J. Chem. Phys. **141**, 234507 (2014).
[37] M.P. Allen and D.J. Tildesley, *Computer Simulation of Liquids* (Oxford University Press, New York, 1987).
[38] H.J.C. Berendsen, J.P.M. Postma, W.F. van Gunsteren, A. DiNola, and J.R. Haak, J. Chem. Phys. **81**, 3684 (1984).
[39] T. Darden, D. York, and L. Pedersen, J. Chem. Phys. **98**, 10089 (1993).
[40] U. Essmann, L. Perera, M.L. Berkowitz, T. Darden, H. Lee, and L.G. Pedersen, J. Chem. Phys. **103**, 8577 (1995).
[41] P.P. Ewald, Ann. Phys. **369**, 253 (1921).
[42] H.J.C. Berendsen, D. van der Spoel, and R. van Drunen, Comput. Phys. Commun. **91**, 43 (1995).
[43] E. Lindahl, B. Hess, and D. van der Spoel, J. Mol. Model. **7**, 306 (2001).
[44] SCAI SuperComputing Application and Innovation, Gromacs Benchmark. http://www.hpc.cineca.it/content/gromacs-benchmark (access date January 25, 2015).
[45] Scalable Software Services for Life Science, Performance Validation and Benchmarking of GROMACS. http://www.scalalife.eu/content/performance-validation-and-benchmarking (access date January 25, 2015).
[46] A. Einstein, Annalen der Physik **322**, 549 (1905).
[47] M. Schoen and C. Hoheisel, Molec. Phys. **52**, 33 (1984).
[48] I.C. Yeh and G. Hummer, J. Phys. Chem. B **108**, 15873 (2004).
[49] G. Guevara-Carrion, J. Vrabec, and H. Hasse, J. Chem. Phys. **134**, 074508 (2011).
[50] R.E. Zeebe, Geochim. Cosmochim. Acta **75**, 2483 (2011).
[51] P. Etesse, J.A. Zega, and R. Kobayashi, J. Chem. Phys. **97**, 2022 (1992).
[52] T. Groß, J. Buchhauser, and H.-D. Lüdemann, J. Chem. Phys. **109**, 4518 (1998).
[53] C.G. Aimoli, E.J. Maginn, and C.R.A. Abreu, J. Chem. Phys. **141**, 134101 (2014).
[54] E.W. Lemmon, M.O. McLinden, D.G. Friend, P.J. Linstrom, and W.G. Mallard, *NIST Chemistry WebBook* (Gaithersburg, MD, 2014).
[55] C. Vega, J.L.F. Abascal, M.M. Conde, and J.L. Aragones, Faraday Discuss. **141**, 251 (2009).
[56] C.G. Aimoli, E.J. Maginn, and C.R.A. Abreu, Fluid Phase Equilib. **368**, 80 (2014).